Salt-induced microheterogeneities in binary liquid mixtures

Markus Bier,[1,2,*] Julian Mars,[3,4] Hailong Li,[3] and Markus Mezger[3,4]

[1]*Max Planck Institute for Intelligent Systems, Heisenbergstrasse 3, 70569 Stuttgart, Germany*

[2]*Institute for Theoretical Physics IV, University of Stuttgart, Pfaffenwaldring 57, 70569 Stuttgart, Germany*

[3]*Max Planck Institute for Polymer Research, Ackermannweg 10, 55128 Mainz, Germany*

[4]*Institute of Physics and MAINZ Graduate School, Johannes Gutenberg University Mainz, Staudingerweg 7, 55128 Mainz, Germany*

(Received 17 May 2017; published 7 August 2017)

The salt-induced microheterogeneity (MH) formation in binary liquid mixtures is studied by small-angle x-ray scattering (SAXS) and liquid state theory. Previous experiments have shown that this phenomenon occurs for antagonistic salts, whose cations and anions prefer different components of the solvent mixture. However, so far the precise mechanism leading to the characteristic length scale of MHs has remained unclear. Here, it is shown that MHs can be generated by the competition of short-ranged interactions and long-ranged monopole-dipole interactions. The experimental SAXS patterns can be reproduced quantitatively by fitting to the derived correlation functions without assuming any specific model. The dependency of the MH structure with respect to ionic strength and temperature is analyzed. Close to the demixing phase transition, critical-like behavior occurs with respect to the spinodal line in the phase diagram.

DOI: 10.1103/PhysRevE.96.022603

I. INTRODUCTION

Structure formation in the bulk of some complex fluids is a well-known phenomenon. Examples include the self-assembly of amphiphiles, block copolymers, room-temperature ionic liquids, or ionic surfactants into micelles, microemulsions, lyotropic phases, or other microscopic heterogeneities [1–9]. There, the structure formation can be easily understood in terms of head-tail asymmetries of the composing molecules or in terms of an asymmetry generated by external fields [10]. Commonly, the different components of the system or molecular groups can be classified in terms of their hydrophilic vs hydrophobic or polar vs apolar character. In most cases, the structural length scales of the systems are then governed by the specific molecular dimensions of these molecular moieties.

However, there are complex fluids that become heterogeneous on length scales well above the molecular dimensions. These fluids comprise binary liquid mixtures in the presence of antagonistic salts, i.e., systems in which cations and anions are preferentially dissolved in different components. Experimentally, indications for microheterogeneity (MH) formation occurred by means of light and small-angle x-ray scattering (SAXS). An additional length scale was first observed in water, 3-methylpyridine, and sodium bromide (NaBr) mixtures [11–13]. A peculiarity of this system is the possible existence of a tricritical point. These studies led to some controversies, which have been resolved by realizing that the postulated MHs were nonequilibrium structures with a long relaxation time [14–16]. Later, small-angle neutron scattering (SANS) provided clear evidence for equilibrium MHs in mixtures of water, 3-methylpyridine, and sodium tetraphenylborate ($NaBPh_4$) [17–21]. In contrast, no pronounced MH could be found for mixtures with inorganic salts [22–29].

Up to now, theoretical studies addressing MH formation have been concentrated on models comprised of a single solvent component [30–32] or a binary mixture solvent in the incompressibility limit [33–37] with dissolved anions and cations. This approach neglects the binary character of the solvent mixture. Thus, MH formation is governed solely by the solvation contrast of the ion species in the solvent. This led to an interpretation where the antagonistic salt ions behave similar to ionic surfactants [19–21]. Recently, this generic approach found some support via SAXS measurements on water, 2,6-dimethylpyridine, and quaternary ammonium bromide salt mixtures [38]. However, there are other systems in which attributing MH formation to solvation contrasts alone [32] does not apply [19–21]. Hence, a full understanding of the underlying MH formation mechanisms has yet to be achieved.

The present work concentrates on an important aspect of this general problem, namely the question about the origin of a characteristic length scale of the MH. Experience tells us that characteristic length scales are typically the result of competing mechanisms, and it is the present goal to identify these for a particular type of system. Here, mixtures of water (H_2O), acetonitrile (ACN, CH_3CN), and the antagonistic salts $NaBPh_4$ or tetraphenylphosphonium chloride (PPh_4Cl) (Sec. II A, Fig. 1) are studied by means of SAXS (Sec. II C). The resulting scattering intensity is analyzed in terms of a generic form derived in Sec. II D. In contrast to previous treatments [30–36], which are based on the intuitive picture of MH formation being generated by long-ranged monopole-monopole interactions between the ions, here long-ranged monopole-dipole interactions are taken into account. Indeed, it is found for the present system that Coulomb interactions between the ions alone cannot account for MH formation, but that monopole-dipole interactions between ions and solvent molecules are decisive for the MH formation. In Sec. III, first the SAXS data are discussed (Sec. III A). Next, the concept of a spinodal line is introduced (Sec. III B) and the critical-like behavior of the system with respect to this spinodal line is verified (Sec. III C). Moreover, the dependence of the characteristic length scale of MHs on the temperature and the ionic strength are determined (Sec. III D). Finally,

*bier@is.mpg.de

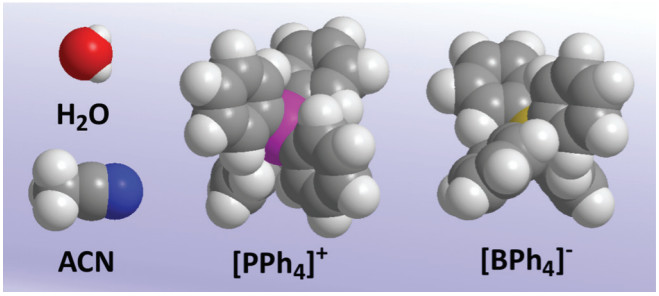

FIG. 1. Molecular structure of the solvent and antagonistic salt components: water (H_2O), acetonitrile (ACN), $[PPh_4]^+$ cations, and $[BPh_4]^-$ anions. Color code: oxygen (red), nitrogen (blue), phosphorus (pink), boron (yellow), carbon (gray), and hydrogen (light gray).

based on the proposed approach accounting for long-ranged monopole-dipole interactions, competing mechanisms, which can give rise to the characteristic length scale of MHs, are propounded in Sec. IV.

II. METHOD AND EXPERIMENTS

A. Setting

The systems under consideration are binary mixtures of polar solvents, denoted as components "A" and "B." The mixture exhibits a miscibility gap with an upper or lower critical demixing point at mole fraction $x_{A,c}$ of component A and temperature T_c. An extensive summary of binary solvent mixtures with lower (LCST) and upper (UCST) critical points was compiled by Francis [39]. In this liquid, univalent ions of an antagonistic salt composed of cations "$\oplus$" and anions "$\ominus$" are dissolved. To experimentally study the MH close to the critical demixing point (T_c,$x_{A,c}$) by SAXS, the system ideally fulfills a series of requirements:

(i) The critical temperature T_c should be in the experimentally accessible temperature range and $x_{A,c} \approx 1/2$.

(ii) Around room temperature, both components should be miscible in all proportions.

(iii) The two components A and B of the mixture should exhibit a good x-ray scattering contrast. In the forward direction, the scattering contrast is quantified by the difference of the real parts $\mathrm{Re}\,(n) = 1 - \delta$ of the refractive indices of the two solvent components. For hard x rays of energy E and soft matter composed of elements from the first or second period, the refractive index decrement $\delta \approx 0.23 \times 10^{-3}\ \frac{\mathrm{cm^3\,keV^2}}{\mathrm{g}}\ \frac{\varrho_\mathrm{m}}{E^2}$ can be estimated from the mass density ϱ_m [40].

(iv) The solubility of the antagonistic salt in the solvent mixture should be $\gtrsim$100 mM. Table I summarizes the relevant parameters of solvents in which MHs have been previously studied experimentally.

TABLE I. Solvent properties of water (H_2O), acetonitrile (ACN), 1,4-dioxane (EDO), 3-methylpyridine (3MP), and 2,6-dimethylpyridine (DMP): melting point T_m [41], mass density ϱ_m [41], refractive index decrement δ for 8 keV x rays [40], electric dipole moment p [41,42], and static dielectric constant ε_r [43].

	T_m (°C)	ϱ_m (g cm^{-3})	δ (10^{-6})	p (D)	ε_r
H_2O	0.0026	0.9982	3.58	1.855	80
ACN	−44	0.7857	2.72	3.925	36
EDO	11.75	1.0337	3.63	<0.4	2.2
3MP	−18.1	0.9566	3.31	2.4	10
DMP	−6.12	0.9226	3.22	1.66	6.9

B. Material system

For the experiments presented in this work, mixtures of water (H_2O) and acetonitrile (ACN) were studied by SAXS (Sec. II C). The system exhibits a miscibility gap with an upper critical demixing point at $x_{\mathrm{H_2O},c} = 0.638$ and $T_c = -1.34\,^\circ$C [44]. Comparison of the H_2O dipole moment (1.855 D) with ACN (3.925 D) renders ACN the more polar component. At 8 keV, the refractive index decrement δ for H_2O ($\delta = 3.58 \times 10^{-6}$) is 32% larger than for ACN ($\delta = 2.72 \times 10^{-6}$). Therefore, compared to water-3MP mixtures used in previous studies [17,19,21,24,25], the water-ACN system provides a much larger scattering contrast in SAXS experiments (Table I). Here, salts with the cations Na^+ or $[PPh_4]^+$ and with the anions Cl^- or $[BPh_4]^-$ were studied. From the Gibbs free energies of transfer $\Delta_t G^\circ(H_2O \rightarrow \mathrm{ACN})$ it is inferred that Na^+ and Cl^- ions prefer H_2O over ACN, whereas $[BPh_4]^-$ and $[PPh_4]^+$ ions prefer ACN over H_2O [45–47]. Thus, $NaBPh_4$ and PPh_4Cl can be considered as antagonistic salts. To verify the importance of the antagonistic character of the salt for MH formation, NaCl with a solubility of 6.1 M in H_2O and 40 μM in ACN served as an example for a hydrophilic salt [48]. In contrast, $[PPh_4][BPh_4]$ has a solubility of 2.72 nM in H_2O and 1.14 mM in ACN [49]. However, its solubility in the mixtures was too low to experimentally study the presence of MH. Measurements were performed for H_2O mole fractions $x_{\mathrm{H_2O}} \in \{0.635, 0.7, 0.8\}$ and ionic strengths $I \in \{10, 50, 200\}$ mM. Purified water was prepared by ultrafiltration and deionization (Sartorius Arium 611 VF, 18.2 MΩ). Other chemicals, namely ACN (Fisher Chemicals, HPLC grade), $NaBPh_4$ (Sigma Aldrich, ⩾99.5%), PPh_4Cl (Sigma Aldrich, ⩾98.0%), and NaCl (Sigma Aldrich, ⩾99.8%), were used as received. The robustness of the results has been verified by repeated preparation and SAXS measurements of some compositions.

C. Small-angle x-ray scattering

SAXS measurements were performed at a self-constructed instrument [50] using a rotating Cu anode x-ray generator (Rigaku MicroMax 007). The beam was monochromatized (wavelength $\lambda = 1.54$ Å) and collimated by a multilayer optic (Osmic Confocal Max-Flux, Cu $K\alpha$) and three four-jaw slit sets (500 × 500 μm^2 slit gap) with 150 cm collimation length. An incident x-ray flux of $\sim 10^7$ photons/s at the sample position was measured by an inversion layer silicon photodiode (XUV-100, OSI Optoelectronics). Samples were contained in 1-mm-thick sealed glass capillaries, placed in a temperature-controlled holder (stability better ±0.05 K), and mounted inside the vacuum chamber. Two-dimensional (2D) diffraction patterns were recorded on an online image plate detector (Mar345). The sample-detector distance of 210 cm

was calibrated with silver behenate [51,52]. SAXS data, collected during three or more independent measurements with 1200 s exposure time each, were averaged and corrected by dark images. Artifacts, originating from high-energy radiation, were removed by differential Laplace filtering. By azimuthal integration, the 2D data sets were converted to scattering intensities $\mathcal{I}(q)$ versus momentum transfer $q = 4\pi/\lambda\ \sin(\vartheta)$ with total scattering angle 2ϑ. To focus on the scattering from MHs, for all data sets the corresponding scattering patterns recorded at 25 °C and constant, q-independent offset values were subtracted from the raw data. This ensures that for sufficiently high q-values, the average intensity $\langle\mathcal{I}(q)\rangle$ vanishes.

D. Generic form of the scattering intensity

To gain physical insight from the measured scattering intensities $\mathcal{I}(q)$, a fitting function is required that allows for an interpretation of the underlying model parameters. The derivation of the fitting function used in the present work is based on a model-free reasoning in terms of the direct correlation functions $c_{ij}(r), i,j \in \{A,B,\oplus,\ominus\}$. This approach is similar to the one employed in Ref. [32].

In a first step, one splits the 3D-Fourier integrals

$$\widehat{c}_{ij}(q) = \frac{4\pi}{q}\int_0^\infty dr\, r c_{ij}(r)\sin(qr) = \widehat{c^<_{ij}}(q) + \widehat{c^>_{ij}}(q) \tag{1}$$

of the direct correlation functions $c_{ij}(r)$ [53] with

$$\widehat{c^<_{ij}}(q) = \frac{4\pi}{q}\int_0^R dr\, r c_{ij}(r)\sin(qr), \tag{2}$$

$$\widehat{c^>_{ij}}(q) = \frac{4\pi}{q}\int_R^\infty dr\, r c_{ij}(r)\sin(qr). \tag{3}$$

As the integration range in Eq. (2) is a compact interval for any finite value R, $\widehat{c^<_{ij}}(q)$ is an even and entire function, i.e., it possesses an expansion of the form

$$\widehat{c^<_{ij}}(q) = c^{<(0)}_{ij} + c^{<(2)}_{ij}q^2 + O(q^4). \tag{4}$$

Short-ranged interactions, e.g., due to solvation, formation of coordination complexes, or hydrogen bonding, contribute only to this part of the direct correlation function, provided the range R is larger than the interaction range.

For sufficiently large R, the direct correlation functions are given by $c_{ij}(r) \simeq -\beta U_{ij}(r)$ at distances $r > R$ with the pair interaction potential $U_{ij}(r)$ of species i and j [53]. As solvent molecules are electrically neutral, i.e., they do not carry an electric monopole; only dipole-dipole interactions are present asymptotically, i.e., $U_{ij}(r > R) \simeq A^{(6)}_{ij}/r^6$ for $i,j \in \{A,B\}$. Note that here "dipole" refers to permanent, induced, or spontaneous dipoles and that permanent dipoles are orientationally disordered. In contrast, the asymptotic interactions at long distances $r > R$ between a solvent molecule and an ion, which by definition carries an electric monopole, are not only of the type monopole-dipole, but additional dipole-dipole contributions (van der Waals forces) occur, i.e., $U_{ij}(r > R) \simeq A^{(4)}_{ij}/r^4 + A^{(6)}_{ij}/r^6$ for $i \in \{A,B\}, j \in \{\oplus,\ominus\}$. Similarly, two ions, both of which carry electric monopoles, interact asymptotically at long distances $r > R$ with monopole-monopole, monopole-dipole, and dipole-dipole contributions, i.e., $U_{ij}(r > R) \simeq A^{(1)}_{ij}/r + A^{(4)}_{ij}/r^4 + A^{(6)}_{ij}/r^6$ for $i,j \in \{\oplus,\ominus\}$ with $A^{(1)}_{ij} = z_i z_j \ell_B/\beta$, $z_\oplus = 1$, $z_\ominus = -1$, and the Bjerrum length $\ell_B = \beta e^2/(4\pi\varepsilon_0\varepsilon)$.

A straightforward expansion of

$$W(\alpha) := \frac{4\pi}{q}\int_R^\infty dr\, r^{1-\alpha}\sin(qr) \tag{5}$$

in powers of q leads to [54]

$$W(1) = 4\pi\left(\frac{1}{q^2} - \frac{R^2}{2} + \frac{R^4}{24}q^2 + O(q^4)\right), \tag{6}$$

$$W(4) = 4\pi\left(\frac{1}{R} - \frac{\pi}{2}q + \frac{R}{6}q^2 + O(q^4)\right), \tag{7}$$

$$W(6) = 4\pi\left(\frac{1}{3R^3} - \frac{1}{6R}q^2 + O(q^3)\right). \tag{8}$$

From Eq. (3) one infers

$$c^>_{ij}(q) = -\beta A^{(6)}_{ij} W(6) \tag{9}$$

for $i,j \in \{A,B\}$,

$$c^>_{ij}(q) = -\beta\left(A^{(4)}_{ij}W(4) + A^{(6)}_{ij}W(6)\right) \tag{10}$$

for $i \in \{A,B\}, j \in \{\oplus,\ominus\}$, and

$$c^>_{ij}(q) = -\beta\left(A^{(1)}_{ij}W(1) + A^{(4)}_{ij}W(4) + A^{(6)}_{ij}W(6)\right) \tag{11}$$

for $i,j \in \{\oplus,\ominus\}$.

Combining the expansions in Eqs. (4) and (9)–(11), one obtains from Eq. (1) the expansions

$$\widehat{c}_{ij}(q) = c^{(0)}_{ij} + c^{(2)}_{ij}q^2 + O(q^3) \tag{12}$$

for $i,j, \in \{A,B\}$,

$$\widehat{c}_{i,j}(q) = c^{(0)}_{ij} + c^{(1)}_{ij}q + c^{(2)}_{ij}q^2 + O(q^3) \tag{13}$$

for $i, \in \{A,B\}, j \in \{\oplus,\ominus\}$, and

$$\widehat{c}_{ij}(q) = -\frac{z_i z_j \ell_B}{q^2} + c^{(0)}_{ij} + c^{(1)}_{ij}q + c^{(2)}_{ij}q^2 + O(q^3) \tag{14}$$

for $i,j \in \{\oplus,\ominus\}$.

The coefficients $c^{(k)}_{ij}$ depend on the system as well as on the thermodynamic state. Note that, due to Eq. (7), nonvanishing coefficients $c^{(1)}_{ij} \neq 0$ can occur only in the presence of long-ranged monopole-dipole interactions.

To calculate the partial structure factors, the 4×4 matrix $\underline{\underline{\mathcal{C}}}$ with components $\mathcal{C}_{ij} := \sqrt{\varrho_i\varrho_j}\,\widehat{c}_{ij}(q)$ is introduced. Here, ϱ_i is the bulk number density of species i. Then, one obtains the matrix $\underline{\underline{\mathcal{S}}} = (\underline{\underline{1}} - \underline{\underline{\mathcal{C}}})^{-1}$, whose components $\mathcal{S}_{ij}$ are related to the partial structure factors $S_{ij}(q) = \sqrt{\varrho_i\varrho_j}\,\mathcal{S}_{ij}/\varrho$, where $\varrho = \sum_i \varrho_i$ denotes the total number density [53]. Here, only wave numbers q corresponding to length scales larger than the molecular sizes are considered, where the form factors of the solvent species $i \in \{A,B\}$ are essentially given by the numbers Z_i of electrons per molecule: $\mathcal{I}(q) \sim \sum_{i,j\in\{A,B\}} Z_i Z_j S_{ij}(q)$.

Performing the matrix inversion in $\underline{\underline{\mathcal{S}}} = (\underline{\underline{1}} - \underline{\underline{\mathcal{C}}})^{-1}$ by means of Cramer's rule, one obtains the following Padé approximation of the scattering intensity in the range of large length scales ($q \to 0$):

$$\mathcal{I}(q) \simeq \frac{aq^2 + bq + c}{q^2 + mq + n}. \tag{15}$$

The coefficients a, b, c, m, and n in Eq. (15) depend on the system and on the thermodynamic state. Given any specific model for the system under consideration, one would obtain explicit expressions of these coefficients. However, within the general approach of the present work, one can merely expect the coefficients a, c, and n in Eq. (15) to be positive. For later reference, the expressions of coefficients m and n are given in the form

$$m = -M\left(c^{(1)}_{\oplus\oplus} + 2c^{(1)}_{\oplus\ominus} + c^{(1)}_{\ominus\ominus} + 2\frac{\left(1-c^{(0)}_{AA}\right)T^{(0)}_B T^{(1)}_B + c^{(0)}_{AB}\left(T^{(0)}_A T^{(1)}_B + T^{(0)}_B T^{(1)}_A\right) + \left(1-c^{(0)}_{BB}\right)T^{(0)}_A T^{(1)}_A}{\left(1-c^{(0)}_{AA}\right)\left(1-c^{(0)}_{BB}\right) - \left(c^{(0)}_{AB}\right)^2}\right) \tag{16}$$

with $T^{(k)}_i := c^{(k)}_{i\oplus} + c^{(k)}_{i\ominus}$ and

$$n = N\left(1 + \frac{I\bar{n}}{\left(1-c^{(0)}_{AA}\right)\left(1-c^{(0)}_{BB}\right) - \left(c^{(0)}_{AB}\right)^2}\right). \tag{17}$$

The positive coefficients M, N, and $\bar{n}$ in Eqs. (16) and (17) are system- and state-dependent. Moreover, M and N vanish in the salt-free case ($I = 0$). Writing the denominator in Eq. (15) in the form $(q + m/2)^2 + n - m^2/4$, one recognizes for $m < 0$ the occurrence of a maximum of $\mathcal{I}(q)$ at $q = q_{\max} := -m/2$ with a peak width of half-height $2/\xi$, where $\xi := 1/\sqrt{n - m^2/4}$.

III. RESULTS AND DISCUSSION

A. Fits of the scattering intensity

Figure 2 displays examples of measured scattering intensities $\mathcal{I}(q)$ (circles) and the corresponding fits according to Eq. (15) (lines) for water mole fraction $x_{H_2O} = 0.635$ at various temperatures T. In Fig. 2(a) the case of a pure, salt-free ($I = 0$) mixture is shown, where $\mathcal{I}(q)$ is monotonically decreasing with a maximum at wave number $q = 0$. The increase of the maximum $\mathcal{I}(0)$ upon decreasing the temperature T is related to the approach of the critical point at $x_{H_2O,c} = 0.638$, $T_c = -1.34\,^\circ$C (Sec. II B). Qualitatively the same monotonically decreasing scattering intensities $\mathcal{I}(q)$ have been observed for all pure, salt-free mixtures as well as for the mixtures with added NaCl.

In contrast, adding one of the antagonistic salts $NaBPh_4$ or PPh_4Cl to an H_2O-ACN mixture results in nonmonotonic scattering intensities $\mathcal{I}(q)$, as is displayed in Fig. 2(b) for $x_{H_2O} = 0.635$ with $I = 50$ mM $NaBPh_4$. Upon decreasing the temperature T, the height of the maxima $\mathcal{I}(q_{\max})$ increases and the wave numbers $q_{\max}$ of the maximum shift toward smaller values. These properties are discussed more systematically in the following sections. The conclusion here is that the occurrence of a peak in the scattering intensity $\mathcal{I}(q)$ at a wave number $q = q_{\max} > 0$, which is related to the formation of a MH of length scale $2\pi/q_{\max}$, is clearly induced by the addition of antagonistic salt.

The formation of salt-induced MHs has been observed already before in mixtures of water and 3-methylpyridine by means of SANS [17,19,21,24,25], and it has been analyzed in terms of a fitting function

$$\mathcal{I}(q) \simeq \frac{I(0)\left(1 + \frac{q^2}{\kappa^2}\right)}{\frac{\xi_0^2}{\kappa^2}q^4 + \left(\frac{1}{\kappa^2} + \xi_0^2(1-g^2)\right)q^2 + 1} \tag{18}$$

with the bulk correlation length ξ_0 of the pure, salt-free ($I = 0$) solvent, the inverse Debye length $\kappa = \sqrt{8\pi\ell_B I}$, and a parameter g^2 describing solubility contrasts of the ions [32,33,36]. It has been shown in Ref. [32] that Eq. (18) is the generic form in the absence of monopole-dipole interactions, i.e., for the case that the structure formation is generated by short-ranged interactions and long-ranged monopole-monopole interactions alone. Attempting to fit Eq. (18) to the SAXS data of the present study of H_2O/ACN mixtures leads to unphysical parameters, such as values of κ^2 that are *negative* and of wrong magnitude. Therefore, the intuitively appealing physical picture underlying Eq. (18) of MH formation due to a competition between short-ranged interactions and Coulomb interactions among the ions does not apply here, and one has to find alternatives. This observation is a clear indication of the importance of monopole-dipole interactions between ions and solvent molecules in understanding the formation of salt-induced MHs in mixtures of H_2O and ACN. Indeed, inspection of Eq. (16) shows that the coefficient m in Eq. (15), and therefore the position $q_{\max} = -m/2$ of the maximum of $\mathcal{I}(q)$, is different from zero only if there are nonvanishing coefficients $c^{(1)}_{ij}$. The coefficients $c^{(1)}_{ij}$, which originate from Eq. (7), describe long-ranged monopole-dipole interactions.

In contrast to the water-ACN system studied in this work, the small-angle scattering patters from water-3MP mixtures [17,19,21,24,25] lead to physically meaningful parameters using Eq. (18). This may be caused by the different ratios between specific interactions present in the two systems. In the general case of nonvanishing monopole-dipole interactions (e.g., water-ACN), it is expected that the scattering patterns $\mathcal{I}(q)$ for binary mixtures of dipolar fluids can be described by Eq. (15). In the case of vanishing or negligible monopole-dipole interactions (e.g., water-3MP), Eq. (18) may apply. However, so far there is currently no theory available that can *a priori* predict from common solvent properties (Table I) whether Eq. (15) or Eq. (18) has to be used.

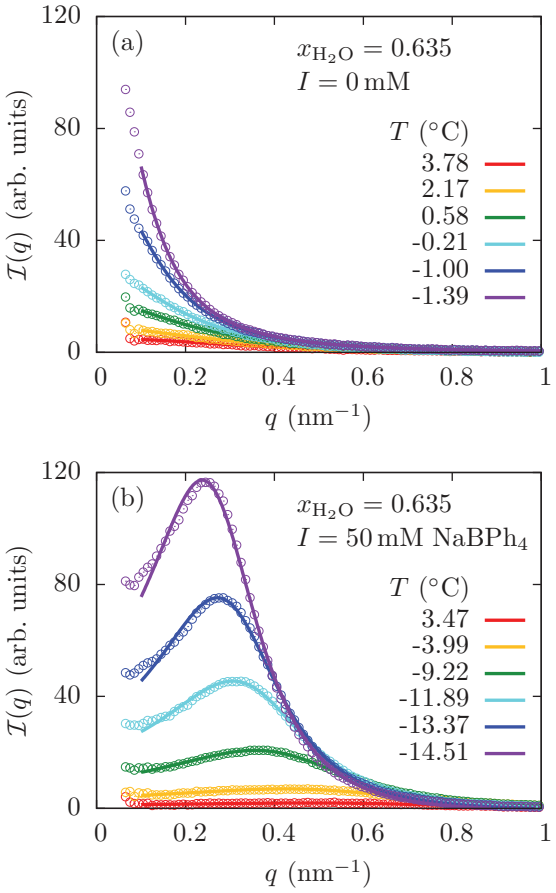

FIG. 2. Scattering intensities $\mathcal{I}(q)$ of binary mixtures of H_2O and ACN for water mole fraction $x_{H_2O} = 0.635$ at various temperatures T. Circles represent the measured SAXS data, whereas lines correspond to fits of Eq. (15). Panel (a) displays the case of the pure, salt-free mixture, which leads to monotonically decaying $\mathcal{I}(q)$ with a maximum at $q = 0$. Panel (b) shows the case of $I = 50$ mM NaBPh$_4$ added to the mixture in panel (a), which exhibits a maximum of $\mathcal{I}(q)$ at wave number $q = q_{max} > 0$. In both panels (a) and (b), the height of the maxima increases upon decreasing the temperature, i.e., upon approaching the two-phase coexistence region in the phase diagram. Moreover, panel (b) shows a decrease of q_{max}, i.e., an increase of the length scale $2\pi/q_{max}$ of the MH, upon decreasing the temperature.

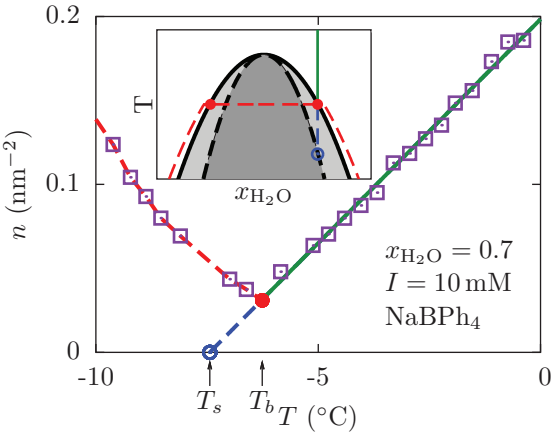

FIG. 3. Parameter n of the generic form Eq. (15) of the scattering intensity $\mathcal{I}(q)$ as a function of the temperature T for water mole fraction $x_{H_2O} = 0.7$ and ionic strength $I = 10$ mM of added NaBPh$_4$. Upon extrapolating (dashed blue line) the linear high-temperature behavior (solid green line), one obtains the spinodal temperature T_s (blue circle). Below the binodal temperature T_b (red dot), the low-temperature behavior (dashed red line) occurs, which corresponds to the phase-separated system.

B. Spinodal line

By fitting Eq. (15) to the measured SAXS data, one obtains the coefficients a, b, c, m, and n as functions of the solvent composition x_{H_2O}, the salt type, the ionic strength I, and the temperature T. Inspection of these dependencies led to the observation of n being a linear function of T for sufficiently high temperatures, as is demonstrated in Fig. 3 by the fitted values of n in the range $T > T_b$ (violet squares with a solid green line underneath). Extrapolation of the linear high-temperature data (dashed blue line) toward $n = 0$ (blue circle) leads to the characteristic temperature T_s and the slope $\mathcal{N}$, by means of which the dashed blue and the solid green lines in Fig. 3 are given as $n(T \geqslant T_s) = \mathcal{N}(T - T_s)$. However, in the low-temperature range $T < T_b$ the fitted values of n (violet squares with a dashed red line underneath) deviate from the extrapolated linear high-temperature behavior with a progressively larger magnitude upon decreasing the temperature.

To interpret this finding, one first infers from Eq. (15) that macroscopic concentration fluctuations $\mathcal{I}(0) = c/n$ are inversely proportional to n and therefore maximal at $T = T_b$. If the measured values of n (violet squares in Fig. 3) followed the linear high-temperature trend $n(T \geqslant T_s) = \mathcal{N}(T - T_s)$ down to $T \searrow T_s$, concentration fluctuations would diverge [$\mathcal{I}(0) \to \infty$]. This suggests the interpretation of $T = T_s(x_{H_2O})$ as the spinodal line in a T-x_{H_2O} phase diagram (dashed black line in the inset of Fig. 3). However, other than exactly at the critical composition $x_{H_2O} = x_{H_2O,c}$, divergence of concentration fluctuations upon decreasing the temperature is preempted by phase separation, which takes place at the binodal line $T = T_b(x_{H_2O})$ in a T-x_{H_2O} phase diagram (solid black line in the inset of Fig. 3). After phase separation has set in (red dots in the inset of Fig. 3), the distance of the two coexisting phases (dashed red lines in the inset of Fig. 3) from the spinodal line increases upon further decreasing the temperature, which leads to a decrease of the concentration fluctuations $\mathcal{I}(0)$.

The dependence of the binodal temperature T_b and of the spinodal temperature T_s on the composition x_{H_2O}, on the ionic strength I, and on the salt type is shown in Table II. For the salt-free ($I = 0$) mixture with $x_{H_2O} = 0.635$, binodal and spinodal temperatures almost coincide, $T_b \approx T_s$, which is in agreement with the fact that this mole fraction is close to the critical concentration $x_{H_2O,c} = 0.638$.

The dependence of the spinodal temperature $T_s(I)$ on the ionic strength I is displayed in Fig. 4 for water mole fraction $x_{H_2O} \in \{0.635, 0.7\}$ and antagonistic salts ("N" $\equiv$ NaBPh$_4$ and "P" $\equiv$ PPh$_4$Cl). Realizing that the denominator on the right-hand side of Eq. (17) measures the macroscopic concentration fluctuations of the salt-free mixture, one expects the scaling

TABLE II. Binodal temperature T_b and spinodal temperature T_s for some systems characterized by water mole fraction $x_{H_2O} \in \{0.635,0.7\}$, ionic strength $I \in \{0,10\}$ mM, and the type of salt ("N"≡ $NaBPh_4$, "P"≡ PPh_4Cl, and a blank space indicating no salt).

x_{H_2O}	0.635	0.635	0.635	0.7	0.7
I (mM)	0	10	10	0	10
Salt		N	P		N
T_b (°C)	−1.34	−6.66	−4.68	−1.55	−6.36
T_s (°C)	−1.36	−7.25	−5.15	−2.26	−7.44

behavior

$$\left(1-c_{AA}^{(0)}\right)\left(1-c_{BB}^{(0)}\right)-\left(c_{AB}^{(0)}\right)^2 \sim [T_s(0)-T]^{\gamma} \qquad (19)$$

in the temperature range $T < T_s(0)$, where $\gamma \approx 1.2372$ is the well-known critical exponent of order-parameter fluctuations of the 3D-Ising universality class [55]. By definition, n vanishes at $T = T_s(I)$, and hence, from Eqs. (17) and (19), one infers $[T_s(0) - T_s(I)]^{\gamma} \sim I$, i.e.,

$$T_s(0) - T_s(I) \sim I^{1/\gamma}. \qquad (20)$$

This scaling behavior is reasonably well confirmed by the experimental data in Fig. 4.

C. Critical-like behavior

Upon approaching the critical point, well-known critical behavior occurs, e.g., the divergence of the concentration fluctuations $\mathcal{I}(0)$ and of the bulk correlation length ξ according to power laws with universal critical exponents [55]. Moreover, the same critical-like behavior can be expected to occur upon approaching the spinodal line $T = T_s(x_{H_2O}, I)$ anywhere, i.e., not only at the critical point.

Figure 5 displays $\mathcal{I}(0) = c/m$ as a function of the temperature difference $T - T_s$ from the spinodal line for solvent composition $x_{H_2O} \in \{0.635,0.7\}$, ionic strength $I \in \{0,10,50,200\}$ mM, and antagonistic salts ("N"≡ $NaBPh_4$ and "P"≡ PPh_4Cl). At small temperature distances $T - T_s$ inside the one-phase region of the phase diagram, i.e., for $T > T_b$, the expected universal scaling behavior $\mathcal{I}(0) \sim (T - T_s)^{-\gamma}$ with the universal critical exponent $\gamma \approx 1.2372$ (Ref. [55]) is confirmed for all systems.

Similarly, Fig. 6 displays $\xi = 1/\sqrt{n - m^2/4}$ as a function of the temperature difference $T - T_s$ from the spinodal line for solvent composition $x_{H_2O} \in \{0.635,0.7\}$, ionic strength $I \in \{10,50,200\}$ mM, and antagonistic salts ("N"≡ $NaBPh_4$ and "P"≡ PPh_4Cl). Again, the expected universal scaling

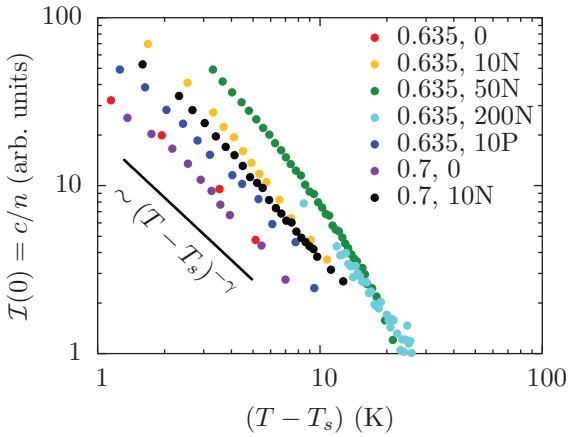

FIG. 5. Macroscopic concentration fluctuations $\mathcal{I}(0)$ for water mole fraction $x_{H_2O} \in \{0.635,0.7\}$, ionic strength $I \in \{0,10,50,200\}$ mM, and some salts ("N"≡ $NaBPh_4$ and "P"≡ PPh_4Cl) as a function of the temperature difference $T - T_s$ from the spinodal. Close to the spinodal, universal critical-like behavior $\mathcal{I}(0) \sim (T - T_s)^{-\gamma}$ with the universal critical exponent γ is observed.

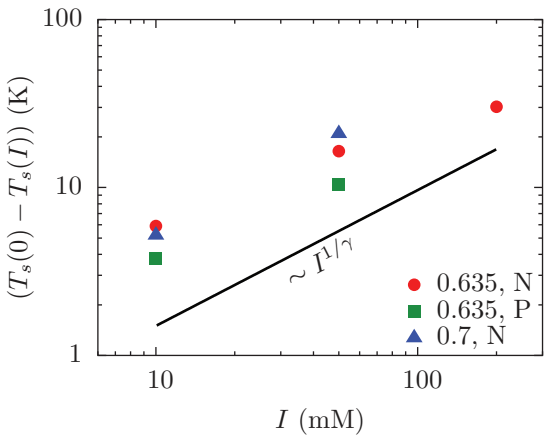

FIG. 4. Dependence of the spinodal temperature T_s (blue circle in Fig. 3) on the ionic strength I for systems with water mole fraction $x_{H_2O} \in \{0.635,0.7\}$ and some antagonistic salts ("N"≡ $NaBPh_4$ and "P"≡ PPh_4Cl). The spinodal temperature $T_s(0)$ for pure, salt-free ($I = 0$) mixtures is displayed in Table II. The scaling relation $T_s(0) - T_s(I) \sim I^{1/\gamma}$ with the universal critical exponent γ can be justified by means of general arguments (see the main text).

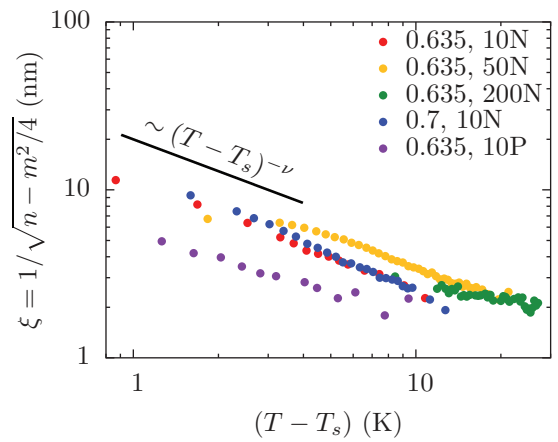

FIG. 6. Correlation length ξ for water mole fraction $x_{H_2O} \in \{0.635,0.7\}$, ionic strength $I \in \{10,50,200\}$ mM, and some salts ("N"≡ $NaBPh_4$ and "P"≡ PPh_4Cl) as a function of the temperature difference $T - T_s$ from the spinodal. Close to the spinodal, universal critical-like behavior $\xi \sim (T - T_s)^{-\nu}$ with the universal critical exponent ν is observed.

behavior $\xi \sim (T - T_s)^{-\nu}$ with the universal critical exponent $\nu \approx 0.6301$ (Ref. [55]) is found.

These results show the consistency of the interpretation of T_s as the spinodal temperature, with respect to which critical-like universality is expected to occur. Moreover, the critical-like behavior found for the present systems belongs to the 3D-Ising universality class. Hence, adding the antagonistic salts $NaBPh_4$ or PPh_4Cl to H_2O + ACN mixtures does not alter the universality class.

D. Structure of microheterogeneities

As already mentioned after Eq. (17), the scattering intensity $\mathcal{I}(q)$ exhibits a maximum at wave number $q = q_{\max} = -m/2$ with a peak width of half-height $2/\xi$. This maximum is related to a characteristic wavelength $2\pi/q_{\max}$ of concentration fluctuations, which decay on the scale of the correlation length $\xi = 1/\sqrt{n - m^2/4}$. Since $\xi \sim (T - T_s)^{-\nu}$, $\nu \approx 0.6301$ (Fig. 6), and $n \sim T - T_s$ (Fig. 3) for $T \searrow T_s$, one expects

$$q_{\max} = -\frac{m}{2} = \sqrt{n - \frac{1}{\xi^2}} \simeq \sqrt{n} = \sqrt{\mathcal{N}}(T - T_s)^{1/2}. \quad (21)$$

This scaling of $q_{\max}$ with respect to $T - T_s$ is confirmed in Fig. 7(a) for solvent composition $x_{H_2O} \in \{0.635, 0.7\}$, ionic strength $I \in \{10, 50, 200\}$ mM, and antagonistic salts ("N"≡ $NaBPh_4$ and "P"≡ PPh_4Cl).

It is found empirically that, given composition x_{H_2O} and salt type, the quantity $q_{\max}/I^{1/4}$ does not depend on the ionic strength I for sufficiently large temperature differences $T - T_s$ from the spinodal, which is shown in Fig. 7(b) for the case $x_{H_2O} = 0.635$ and $NaBPh_4$. Consequently, at sufficiently high temperatures T above the spinodal temperature T_s, the wave number at the peak position $q_{\max}$ scales as $q_{\max} \sim I^{1/4}$.

IV. CONCLUSION AND SUMMARY

All H_2O/ACN mixtures with different concentrations of the two antagonistic salts $NaBPh_4$ and PPh_4Cl exhibit MHs with characteristic length scales in the nm regime. It turned out that MH formation in these systems cannot be attributed to monopole-monopole interactions between the ions alone, but that monopole-dipole interactions between ions and solvent molecules are necessary for a quantitative understanding. By taking into account electric monopole-dipole interactions, a generic form of the SAXS pattern $\mathcal{I}(q)$ has been derived (Sec. II D). Using Eq. (15), the experimental SAXS data can be quantitatively reproduced by fitting (Fig. 2). The resultant quantities are as follows: The amplitude of the macroscopic concentration fluctuations (Fig. 5), the bulk correlation length (Fig. 6), and the characteristic periodicity of the MH [Fig. 7(a)]. In contrast to the parameters extracted by fitting Eq. (18), i.e., the standard model for MHs, those obtained by fitting Eq. (15) are all physically meaningful. Detailed analysis showed that their temperature dependence is governed by the distance from the spinodal line $T = T_s(x_{H_2O}, I)$ in the phase diagram (Fig. 3). Upon adding salt, the spinodal line shifts to lower temperatures (Fig. 4).

A physical understanding of the mechanisms leading to MH formation caused by monopole-dipole interactions is obtained by analysis of Eq. (16). Its relevance is given by the relation

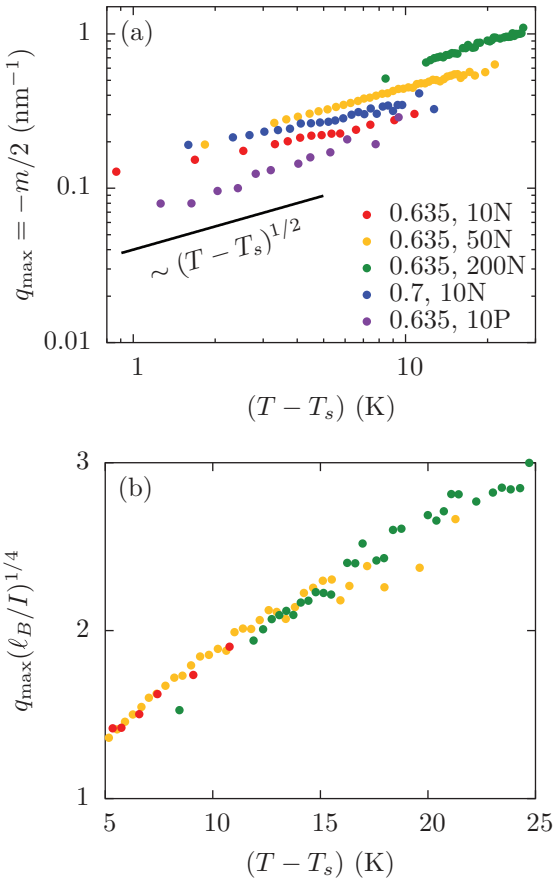

FIG. 7. Dependence of the wave number $q_{\max}$ of the maximum of the scattering intensity $\mathcal{I}(q)$ (Fig. 2) as function of the temperature difference $T - T_s$ from the spinodal for water mole fraction $x_{H_2O} \in \{0.635, 0.7\}$, ionic strength $I \in \{0, 10, 50, 200\}$ mM, and some salts ("N"≡ $NaBPh_4$ and "P"≡ PPh_4Cl). The wave number $q_{\max}$ is related to the characteristic length scale $2\pi/q_{\max}$ of the MH. Panel (a) confirms the scaling $q_{\max} \sim (T - T_s)^{1/2}$ for small temperature differences $T - T_s$ from the spinodal derived in the main text. The collapse of the data points onto one curve in panel (b) shows the scaling $q_{\max} \sim I^{1/4}$ with the ionic strength I for sufficiently large temperature differences $T - T_s$ from the spinodal.

of m to the wave number $q_{\max} = -m/2$ of the MH. The coefficients $c_{ij}^{(1)}$ in Eq. (16) originate exclusively from the long-ranged part of the monopole-dipole interaction [Eq. (7)]. Typically, induced dipoles are much weaker than permanent ones. Therefore, expression $c_{\oplus\oplus}^{(1)} + 2c_{\oplus\ominus}^{(1)} + c_{\ominus\ominus}^{(1)}$ in Eq. (16) can be neglected. The dominant last term in the large parentheses of Eq. (16) may be rewritten in order to obtain

$$q_{\max} \approx M \begin{pmatrix} T_A^{(0)} \\ T_B^{(0)} \end{pmatrix} \begin{pmatrix} 1 - c_{AA}^{(0)} & -c_{AB}^{(0)} \\ -c_{AB}^{(0)} & 1 - c_{BB}^{(0)} \end{pmatrix}^{-1} \begin{pmatrix} T_A^{(1)} \\ T_B^{(1)} \end{pmatrix}. \quad (22)$$

The inverse matrix in Eq. (22) corresponds to the partial structure factors $\underline{\underline{S}}^{(0)}$ of the pure, salt-free mixture at wave number $q = 0$. Hence, due to Yvon's equation [53], it is proportional to the integral of the density-density correlation matrix $\underline{\underline{\widehat{G}}}^{(0)} = \varrho \underline{\underline{S}}^{(0)}$. Therefore, Eq. (22) expresses the scenario in which MHs with $q_{\max} \neq 0$ originate from a coupling

(represented by $\underline{\underline{\widehat{G}}}^{(0)}$) of short-ranged interactions (represented by $\underline{T}^{(0)}$) and long-ranged monopole-dipole salt-solvent interactions (represented by $\underline{T}^{(1)}$). It is important to note that $T_i^{(k)} := c_{i\oplus}^{(k)} + c_{i\ominus}^{(k)}, i \in \{A,B\}, k \in \{0,1\}$, is the *sum* of cation-solvent and anion-solvent contributions. In contrast, the scenario described in Refs. [32,33,36] is based on the *differences* between the cation-solvent and anion-solvent interactions.

Based on these formal results, the following picture emerges: A competing mechanism between charge fluctuations and their monopole-dipole interaction leads to the formation of MHs. For an antagonistic salt, the ion species are preferably solvated by different solvent components. The difference is generated by short-ranged interactions, leading to short-ranged correlations only. The preference of antagonistic ions for different solvent components leads to solvation-induced short-ranged charge-density fluctuations, which give rise to long-ranged monopole-dipole interactions. These long-ranged interactions are strongest for the more polar solvent component. The relative strength of short-ranged interactions and long-ranged monopole-dipole interactions determines the characteristic length scale $2\pi/q_{\max}$ of these MHs: The stronger the long-ranged monopole-dipole interaction is, the larger is $q_{\max}$ [Eq. (16) or (22)], i.e., the smaller the characteristic length scale of the MH.

Recently, it has been argued that the absence of MH in H_2O/3MP mixtures with simple inorganic salts [17,19,21,24,25] may be caused by similar anion and cation sizes [32]. However, there the considered inorganic salts are not antagonistic. Within the picture proposed above, the absence of MH can therefore also be understood by a different mechanism: The absence of charge fluctuations leads to vanishing long-ranged monopole-dipole interactions. Accordingly, in the present study, H_2O/ACN mixtures with $I \in \{10,50\}$ mMNaCl exhibit no MH. This observation is in agreement with the findings of Takamuku *et al.* [22,23,26–29].

In summary, salt-induced MHs in H_2O/ACN mixtures with the antagonistic salts $NaBPh_4$ or PPh_4Cl have been systematically studied by SAXS. A detailed analysis of these data suggests that these MHs are generated by a competition of short-ranged interactions and long-ranged electrostatic monopole-dipole interactions. Besides being consistent with the present and previous experimental results, this picture offers an explanation for the occurrence of characteristic length scales of MHs.

In chemical reactions, microheterogeneous solvent structures can influence their catalytic activity. These processes in a macroscopically homogeneous liquid phase can be described as phase transfer or interfacial reactions at domain boundaries [56]. Therefore, the possibility of MH formation with controlled length scales using near-critical solvent mixtures with ionic impurities might offer an attractive approach to tune catalytic reactions. Being partly of electrostatic origin, salt-induced MHs in fluids may be used for pattern formation at interfaces. Here, the electrodes could serve to control the pattern's size and morphology. Detailed studies on such salt-induced MH at interfaces are planned for future investigations.

ACKNOWLEDGMENTS

The authors acknowledge H. Weiss, S. Geiter, X. Wu, and G. Kircher from MPI-P for their help with SAXS measurements and sample preparation, as well as A. Onuki for useful comments. J.M. and M.M. acknowledge the MAINZ Graduate School of Excellence, funded through the Excellence Initiative (DFG/GSC 266), for financial support. H.L. was supported by the China Scholarship Council.

[1] Y. Moroi, *Micelles* (Springer, New York, 1992).
[2] J. Zhang, Z. Wang, J. Liu, S. Chen, and G. Liu, *Self-Assembled Nanostructures* (Kluwer Academic, New York, 2003).
[3] A. M. Figueiredo Neto and S. R. A. Salinas, *The Physics of Lyotropic Liquid Crystals* (Oxford University Press, Oxford, 2005).
[4] *Block Copolymers in Nanoscience*, edited by M. Lazzari, G. Liu, and S. Lecommandoux (Wiley, Weinheim, 2006).
[5] T. G. Mason, J. N. Wilking, K. Meleson, C. B. Chang, and S. M. Graves, J. Phys.: Condens. Matter **18**, R635 (2006).
[6] *Self-Organized Morphology in Nanostructured Materials*, edited by K. Al-Shamery and J. Parisi (Springer, Berlin, 2008).
[7] *Microemulsions*, edited by C. Stubenrauch (Wiley, Chichester, 2009).
[8] A. H. E. Müller and O. Borisov, *Self Organized Nanostructures of Amphiphilic Block Copolymers* (Springer, Heidelberg, 2011), Vols. I and II.
[9] S. Bier, N. Gavish, H. Uecker, and A. Yochelis, Phys. Rev. E **95**, 060201 (2017).
[10] Y. Tsori and L. Leibler, Proc. Natl. Acad. Sci. USA **104**, 7348 (2007).
[11] J. Jacob, A. Kumar, M. A. Anisimov, A. A. Povodyrev, and J. V. Sengers, Phys. Rev. E **58**, 2188 (1998).
[12] J. Jacob, A. Kumar, S. Asokan, D. Sen, R. Chitra, and S. Mazumder, Chem. Phys. Lett. **304**, 180 (1999).
[13] M. A. Anisimov, J. Jacob, A. Kumar, V. A. Agayan, and J. V. Sengers, Phys. Rev. Lett. **85**, 2336 (2000).
[14] A. F. Kostko, M. A. Anisimov, and J. V. Sengers, Phys. Rev. E **70**, 026118 (2004).
[15] M. Wagner, O. Stanga, and W. Schröer, Phys. Chem. Chem. Phys. **6**, 580 (2004).
[16] J. Leys, D. Subramanian, E. Rodezno, B. Hammoudad, and M. A. Anisimov, Soft Matter **9**, 9326 (2013).
[17] K. Sadakane, H. Seto, H. Endo, and M. Shibayama, J. Phys. Soc. Jpn. **76**, 113602 (2007).
[18] K. Sadakane, A. Onuki, K. Nishida, S. Koizumi, and H. Seto, Phys. Rev. Lett. **103**, 167803 (2009).
[19] K. Sadakane, N. Iguchi, M. Nagao, H. Endo, Y. B. Melnichenko, and H. Seto, Soft Matter **7**, 1334 (2011).
[20] K. Sadakane, M. Nagao, H. Endo, and H. Seto, J. Chem. Phys. **139**, 234905 (2013).
[21] K. Sadakane, H. Endo, K. Nishida, and H. Seto, J. Solution Chem. **43**, 1722 (2014).

[22] T. Takamuku, A. Yamaguchi, D. Matsuo, M. Tabata, M. Kumamoto, J. Nishimoto, K. Yoshida, T. Yamaguchi, M. Nagao, T. Otomo, and T. Adachi, J. Phys. Chem. B **105**, 6236 (2001).
[23] T. Takamuku, A. Yamaguchi, D. Matsuo, M. Tabata, T. Yamaguchi, T. Otomo, and T. Adachi, J. Phys. Chem. B **105**, 10101 (2001).
[24] K. Sadakane, H. Seto, and M. Nagao, Chem. Phys. Lett. **426**, 61 (2006).
[25] K. Sadakane, H. Seto, H. Endo, and M. Kojima, J. Appl. Crystallogr. **40**, s527 (2007).
[26] T. Takamuku, Y. Noguchi, M. Nakano, M. Matsugami, H. Iwase, and T. Otomo, J. Ceram. Soc. Jpn. **115**, 861 (2007).
[27] T. Takamuku, Y. Noguchi, E. Yoshikawa, T. Kawaguchi, M. Matsugami, and T. Otomo, J. Mol. Liq. **131-132**, 131 (2007).
[28] T. Takamuku, Y. Noguchi, M. Matsugami, H. Iwase, T. Otomo, and M. Nagao, J. Mol. Liq. **136**, 147 (2007).
[29] H. Haramaki, T. Shimomura, T. Umecky, and T. Takamuku, J. Phys. Chem. B **117**, 2438 (2013).
[30] V. M. Nabutovskii, N. A. Nemov, and Y. G. Peisakhovich, Phys. Lett. A **79**, 98 (1980).
[31] V. M. Nabutovskii, N. A. Nemov, and Y. G. Peisakhovich, Mol. Phys. **54**, 979 (1985).
[32] M. Bier and L. Harnau, Z. Phys. Chem. **226**, 807 (2012).
[33] A. Onuki and H. Kitamura, J. Chem. Phys. **121**, 3143 (2004).
[34] A. Onuki, R. Okamoto, and T. Araki, Bull. Chem. Soc. Jpn. **84**, 569 (2011).
[35] A. Onuki and R. Okamoto, Curr. Opin. Colloid Interface Sci. **16**, 525 (2011).
[36] M. Bier, A. Gambassi, and S. Dietrich, J. Chem. Phys. **137**, 034504 (2012).
[37] A. Onuki, S. Yabunaka, T. Araki, and R. Okamoto, Curr. Opin. Colloid Interface Sci. **22**, 59 (2016).
[38] M. Witala, S. Lages, and K. Nygård, Soft Matter **12**, 4778 (2016).
[39] A. Francis, Adv. Chem. **31**, 1 (1961).
[40] B. Henke, E. M. Gullikson, and J. C. Davis, At. Data. Nucl. Data Tables **54**, 181 (1993).
[41] W. M. Haynes, *CRC Handbook of Chemistry and Physics* (CRC, Boca Raton, FL, 2017).
[42] J. W. Williams, J. Am. Chem. Soc. **52**, 1838 (1930).
[43] C. Wohlfarth, in *Landolt-Börnstein—Group IV Physical Chemistry 17 (Supplement to IV/6)*, edited by M. D. Lechner (Springer, Berlin, 2008).
[44] J. Szydłowski and M. Szykułar, Fluid Phase Equilib. **154**, 79 (1999).
[45] Y. Marcus, Pure Appl. Chem. **55**, 977 (1983).
[46] H. D. Inerowicz, W. Li, and I. Persson, J. Chem. Soc. Faraday Trans. **90**, 2223 (1994).
[47] C. Kalidas, G. Hefter, and Y. Marcus, Chem. Rev. **100**, 819 (2000).
[48] J. Burgess, *Metal Ions in Solution* (Ellis Horwood, New York, 1978).
[49] O. Popovych, *Solubility Data Series, Volume 18, Tetraphenylborates* (Pergamon, Oxford, 1981).
[50] H. Weiss, J. Mars, H. Li, G. Kircher, O. Ivanova, A. Feoktystov, O. Soltwedel, M. Bier, and M. Mezger, J. Phys. Chem. B **121**, 620 (2017).
[51] T. C. Huang, H. Toraya, T. N. Blanton, and Y. Wu, J. Appl. Crystallogr. **26**, 180 (1993).
[52] R. Gilles, U. Keiderling, and A. Wiedenmann, J. Appl. Crystallogr. **31**, 957 (1998).
[53] J.-P. Hansen and I. R. McDonald, *Theory of Simple Liquids* (Academic, London, 1986).
[54] I. S. Gradshteyn and I. M. Ryzhik, *Table of Integrals, Series, and Products* (Academic, New York, 1980).
[55] A. Pelissetto and E. Vicari, Phys. Rep. **368**, 549 (2002).
[56] O. Hollóczki, A. Berkessel, J. Mars, M. Mezger, A. Wiebe, S. R. Waldvogel, and B. Kirchner, ACS Catal. **7**, 1846 (2017).